Ann. N.Y. Acad. Sci. ISSN 0077-8923

ANNALS OF THE NEW YORK ACADEMY OF SCIENCES
Issue: *Analysis of Cardiac Development*

Noninvasive imaging of cardiac electrophysiology and arrhythmia

Yoram Rudy

Cardiac Bioelectricity and Arrhythmia Center, Washington University in St. Louis, St. Louis, Missouri, USA

Address for correspondence: Prof. Yoram Rudy, Ph.D., Cardiac Bioelectricity and Arrhythmia Center, Washington University in St. Louis, Whitaker Hall, Rm. 290, Campus Box 1097, One Brookings Drive, St. Louis, MO 63130. rudy@wustl.edu

Cardiac arrhythmias are a major cause of death and disability. Despite the clinical need and the importance of studying arrhythmia mechanisms in humans, a noninvasive imaging modality for cardiac electrophysiology is not yet available for routine application. Here we describe such a noninvasive imaging modality, electrocardiographic imaging (ECGI), and provide examples of its application in various (normal and abnormal) cardiac rhythms.

Keywords: cardiac arrhythmias; ECG; imaging

Introduction

An estimated 400,000 people die annually in the United States alone from cardiac rhythm disorders (7 million worldwide). Yet, a noninvasive imaging modality for cardiac electrophysiology and arrhythmias, equivalent to CT or MRI, is not available for clinical practice or human research. Such method is needed for identifying patients at risk of arrhythmia and sudden death, for providing specific diagnosis, and for guiding therapy and assessing its outcome. It is also needed for mechanistic studies of arrhythmias in humans, where the arrhythmogenic substrate is very different from the substrate in animal models.

Electrocardiographic imaging (ECGI) is a noninvasive imaging modality developed in our laboratory.[1] It noninvasively images potentials, electrograms, activation sequences (isochrones), and repolarization patterns on the epicardial surface of the heart. ECGI was extensively validated in animal experiments[2–6] and by comparison to direct cardiac mapping in patients undergoing open heart surgery.[7] In this workshop proceeding I will summarize the ECGI method and provide selected examples of its application in humans. The material presented here was adapted and compiled from my previous publications, referred to in each sub-section.

Methodology

We use 250 electrodes mounted on strips (or organized into a vest) to record 250 electrocardiograms from the entire torso surface. Following the ECG recordings, the patient undergoes a thoracic CT scan with the electrodes in position. The CT images provide the positions of the ECG electrodes and the heart-surface geometry in the same reference frame. The ECGs are the electrical input data and the CT scans are the geometry input data for ECGI. These data are combined in a mathematical algorithm to compute epicardial potentials, electrograms (typically at 600 locations), isochrones, and repolarization patterns. Figure 1 is a diagram of the ECGI procedure. Protocols were reviewed and approved by the Institutional Review Boards (IRBs) at University Hospitals of Cleveland and Washington University in St. Louis.

Computation of potentials on the epicardial surface of the heart from potentials measured on the body surface is based on solving Laplace's equation in the volume between the torso and epicardial surfaces.[8] An integral formulation of this problem (Green's Second Theorem) and the boundary element method (BEM)[9] are used to discretize the problem and derive a matrix A that relates the torso potentials vector V_T to the vector of epicardial potentials V_E: $V_T = AV_E$. The A matrix provides the

doi: 10.1111/j.1749-6632.2009.05103.x

Ann. N.Y. Acad. Sci. 1188 (2010) 214–221

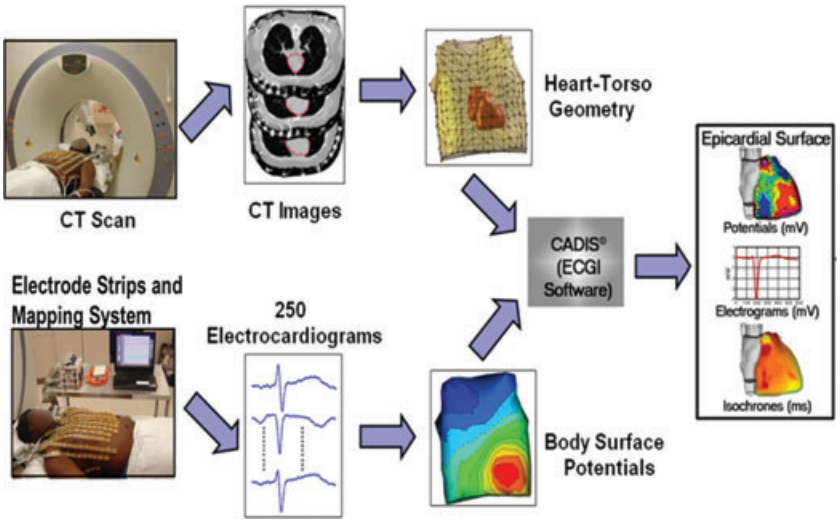

Figure 1. The ECGI procedure: Body surface potential maps (BSPMs) are recorded using a multichannel (250-electrode) mapping system. Non-contrast CT images with the body surface ECGI electrodes applied, simultaneously record the locations of the electrodes (*shining dots* in CT images) and the geometry of the heart surface. By combining the BSPM and heart–torso geometry information, ECGI reconstructs potential maps, electrograms, isochrones (activation patterns), and repolarization patterns on the epicardial surface of the heart. (Modified from Ramanathan *et al.*[1])

heart-torso geometrical relationship obtained using CT. The goal of ECGI is to invert the above equation and computer V_E from the measured V_T. Unfortunately, this "inverse problem" is ill-posed in the sense that small errors and noise in the recorded ECGs can cause large, unbounded errors in the computed epicardial potentials. To overcome this difficulty, we used Tikhonov regularization methods[10] or the Generalized Minimal Residual (GMRes) iterative approach[11] to stabilize the solution. Once epicardial potentials are computed for the entire cardiac cycle (or many cycles) with temporal resolution of 1 ms, they are used to compute epicardial electrograms (potential over time) at 600 epicardial locations. From the electrograms, activation times are determined by the steepest negative deflection on the QRS and isochrones are constructed by connecting sites of equal activation times. Similarly, recovery (repolarization) times are determined as the time of steepest positive deflection on the T-wave.

Selected examples of ECGI images

Normal ventricular activation

Normal ventricular activation[1,12] (sinus rhythm, SR) is characterized by broad activation fronts that propagate from endocardium to epicardium. Epicardial breakthrough occurs when a portion of the wave front reaches the epicardial surface, an event that generates a local epicardial potential minimum. The locations and relative times of various breakthroughs provide important information on the sequence of ventricular activation and its deviation from normal SR in disease states. Figure 2A (left) shows body surface potentials 35 ms after QRS onset during SR in a healthy young adult. Figure 2A (right) is the corresponding ECGI potential map on the epicardial surface of the heart. Several potential minima (dark blue and yellow, numbered 1, 2, 3, 4) indicate breakthrough sites. The earliest breakthrough occurs at the thinnest portion of the right ventricular (RV) free wall (site 1); it is termed "RV breakthrough." The RV breakthrough minimum appears at 22 ms after QRS onset and intensifies at 35 ms. Several breakthrough minima appear on the left ventricular (LV) epicardium (sites 2, 3, and 4). Site 2 is a breakthrough of an activation front generated by the left anterior fascicular branch of the left bundle branch of the specialized conduction system. The minima imaged at sites 1 and 2 are consistent with directly recorded minima at corresponding locations in chimpanzee hearts.[13]

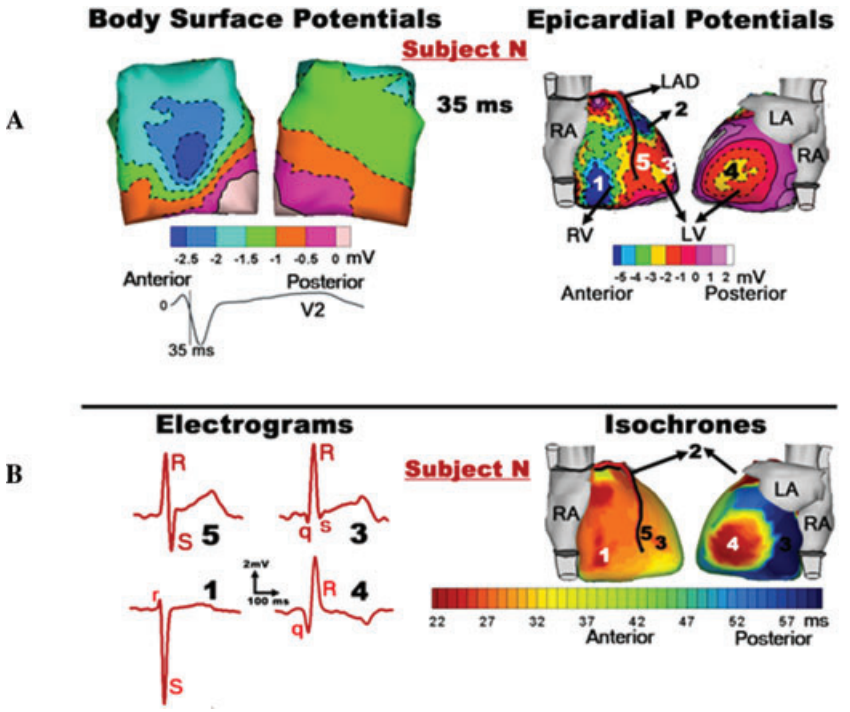

Figure 2. Ventricular activation of a normal subject. (**A**) *Left*: anterior and posterior views of body surface potential map (BSPM), 35 ms after QRS onset. ECG lead 2 is shown for timing. *Right*: noninvasive epicardial potential map reconstructed from BSPM at left. RV, right ventricle; LV, left ventricle; LAD, left anterior descending coronary artery; LA, left atrium; RA, right atrium. (**B**) *Left:* epicardial electrograms from locations 1, 5, 3, and 4 (shown in A [*right*]). *Right*: epicardial isochrones. 1, 2, 3, and 4 indicate locations of early epicardial activation (breakthrough sites). (From Ramanathan *et al.*[1] Reproduced by permission.)

Site 3 is at the LV apex and site 4 in the posterior paraseptal region of the LV. Invasive direct mapping detected the occurrence of all four epicardial breakthroughs, confirming the noninvasive images of ECGI.[14]

Figure 2B (left) shows selected ECGI electrograms from epicardial sites 1, 3, 4, and 5. These human electrograms are very similar in morphology to those directly measured from corresponding locations in the chimpanzee heart. There is a typical progression of electrogram morphology from RV to LV; electrogram 1 is mostly negative, electrograms 4 and 5 are biphasic and electrogram 3 is mostly positive. ECGI also reconstructs well epicardial electrogram T-waves, reflecting the local repolarization process. Anterior RV T-wave is positive (site 1), while at posterior LV (site 4) T-wave is inverted (negative). From the ECGI electrograms, activation-recovery intervals are computed with a typical value of 240 ms, which closely corresponds to measured action-potential durations in ventricular cells and tissue. Figure 2B (right) shows ECGI activation (isochrone) maps during normal SR. Earliest activation is at the four epicardial breakthrough sites of Figure 2A. Latest activation occurs at the posterobasal LV (dark blue, posterior).

Atrial flutter

Figure 3 is an ECGI image of atrial activation isochrones in a patient with chronic atrial flutter.[15] The anterior view shows the reentry circuit that drives the flutter (black arrows). The circuit is confined to the right atrium (RA) and the wave front circulates in the counterclockwise direction. It propagates up the inter-atrial septum (dashed arrow) to emerge near Bachman's bundle (asterisk). It then pivots counterclockwise and propagates down the RA free wall to reenter the septum through the

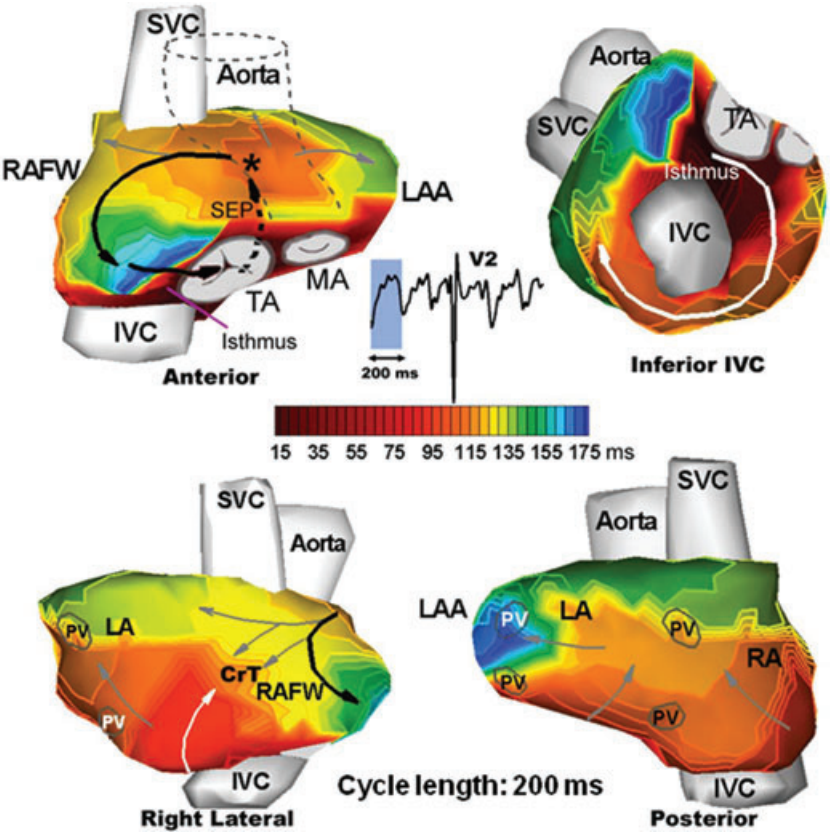

Figure 3. ECGI Images of atrial flutter. Isochrone maps are shown. The right atrial reentry circuit that drives the flutter is indicated by *black arrows*, RAFW, right atrial free wall; LAA, left atrial appendage; SVC, superior vena cava; TA, tricuspid annulus; MA, mitral annulus; PV, pulmonary vein; SEP, septum; CrT, crista terminalis. (From Ramanathan *et al.*[1] Reproduced by permission.)

narrow isthmus between the inferior vena cava and tricuspid annulus (TA). This primary reentry circuit generates many secondary excitatory waves that spread in all directions. A major wave (white arrows) propagates around the IVC (inferior IVC view) and ascends the lateral RA (right lateral view) to the crista terminalis region, where it collides with another front (gray arrows) that emerges from the main reentry circuit in the leftward direction. Other wave fronts (gray arrows in posterior, anterior and right lateral views) emanate from the reentry circuit and propagate to the left atrium (LA), reaching the LA appendage last. The ECGI imaged reentry circuit and details of the atrial activation pattern are consistent with direct catheter mapping of typical atrial flutter in patients.[16–18]

Wolff–Parkinson–White (WPW) syndrome and cardiac memory

The WPW syndrome[19,20] is associated with long-standing abnormal sequence of ventricular activation due to pre-excitation via an atrioventricular accessory pathway (AP).[21] Cardiac memory (CM)[22,23] is defined as persistence of repolarization abnormalities secondary to abnormal activation after normal activation has been restored. Figure 4 shows ECGI epicardial isochrones of a WPW patient pre-ablation of the AP and 45 min post-ablation. Before ablation (left panel) the area of earliest activation (pre-excitation from the AP) is at the base (red; the initiation site is marked with an asterisk). After ablation (right panel) the sequence is reversed and

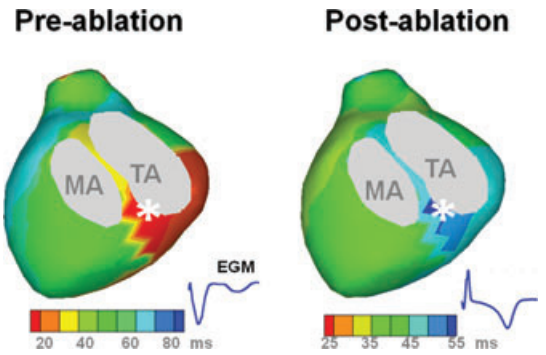

Figure 4. ECGI-imaged epicardial activation maps in a patient with WPW syndrome. *Left:* pre-ablation; *right:* post-ablation. Electrogram (EGM) from the pre-excitation region is also shown. (Adapted from Ghosh *et al.*,[19] with permission.)

this region is activated last (blue) as during normal sinus rhythm. Epicardial electrogram from the pre-excitation region (EGM) shows a negative Q-wave pre-ablation; it is reversed in polarity to a positive R-wave post-ablation. Note that the T-wave is negative pre-ablation and remains negative post-ablation, suggesting presence of CM.

Figure 5 shows repolarization activation–recovery (ARI) maps pre-ablation and at progressive times (45 min, 1 week, 1 month) post-ablation. ARI is a surrogate of the local action potential duration. EGMs from the pre-excitation region are also shown. The QRS complex, reflecting activation, reverses from negative to positive immediately after ablation and remains positive at all later times. In contrast, the T-wave is negative pre-ablation and remains so at 45 min and 1 week post-ablation. Only at 1 month after ablation the T-wave becomes positive. ARIs from the pre-excitation region (350 ms) are greatly prolonged relative to typical ARIs of 300 ms from this region during normal sinus rhythm. At the apex ARI = 240 ms, same as normal, and the base-to-apex ARI gradient pre-ablation is 110 ms. It remains steep at 114 ms 45 min post-ablation and gradually decreases to 80 ms at 1 week and to 40 ms (same as normal) at 1 month. Thus, abnormal repolarization persists post-ablation and gradually returns to normal over one month, exhibiting long-term memory with a time course consistent with transcriptional reprogramming and remodeling of ion channels.

Heart failure and cardiac resynchronization therapy

In more than 30% of advanced heart failure cases, LV activation is delayed. To restore synchrony of contraction, biventricular (BiV) pacing has been applied as a therapeutic approach termed cardiac resynchronization therapy (CRT).[24] We applied ECGI in eight patients with heart failure during native rhythm (NR) and BiV. Figure 6 shows epicardial isochrones during NR in four of the patients. RV activation is consistent with that imaged in the normal heart, with epicardial activation spreading uniformly from an anterior breakthrough site. RV breakthrough occurs 29 $\pm$ 7 ms after onset of the body surface QRS. Duration of the entire RV activation following the breakthrough is 25 $\pm$ 12 ms. In contrast, LV activation is greatly delayed, mostly due to line(s)/region(s) of conduction block in anterior LV that prevent the RV activation front from crossing directly to the LV. The activation front circumvents the block via apical or inferior LV, activating the lateral LV base last in most patients (although there is inter-patient variability in the region of latest activation; see Figure 6 [dark blue area]).

BiV pacing generates very different activation sequences in different patients, with variable degree of resynchronization (not shown). Activation of lateral LV is advanced in all patients, who had lateral LV

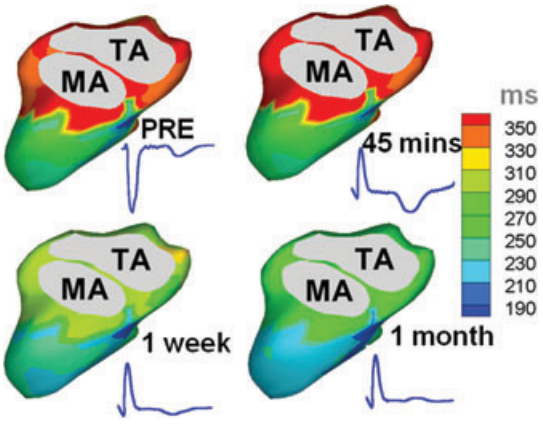

Figure 5. Epicardial activation–recovery interval (ARI) maps pre-ablation and at different times (45 mins, 1 week, and 1 month) post-ablation. EGM from pre-excitation region is also shown. MA, mitral annulus; TA, tricuspid annulus. (Modifed from Ghosh *et al.*[19])

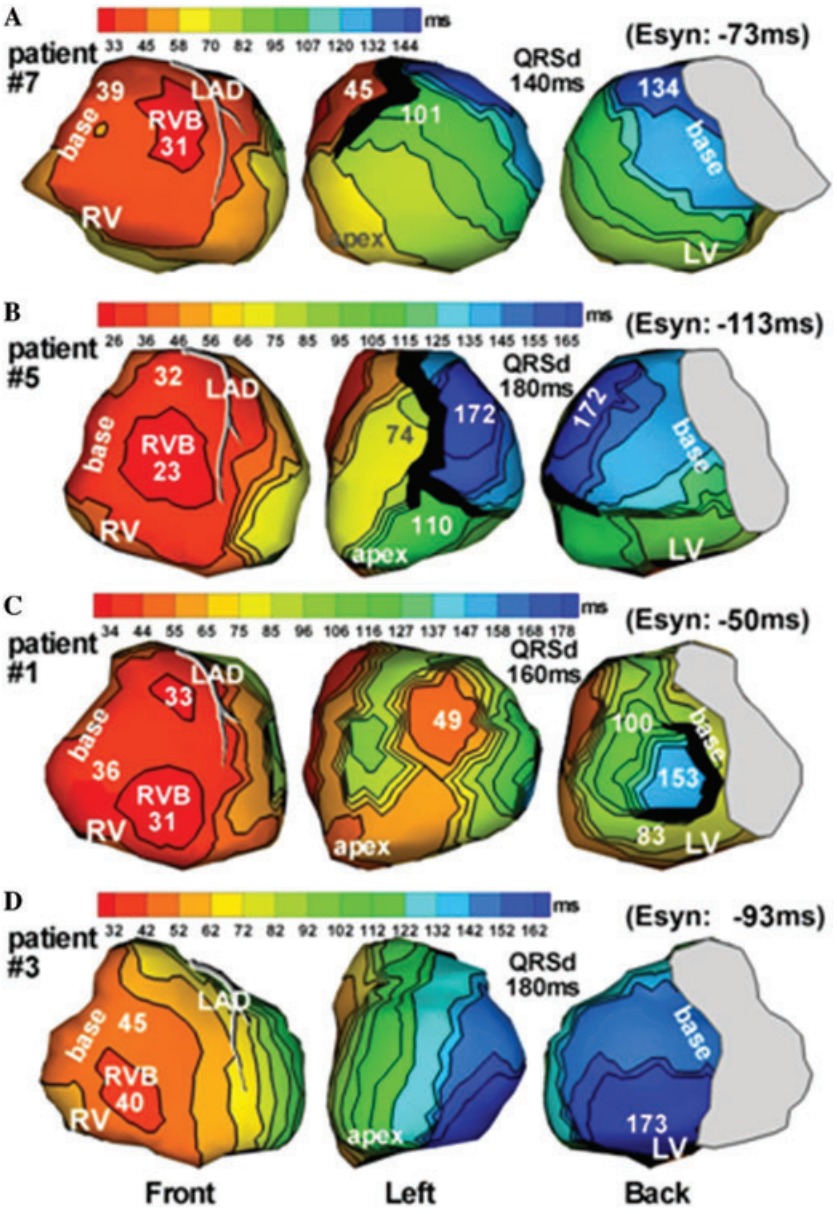

Figure 6. **Activation maps during native rhythm in four patients with heart failure. Thick black markings indicate conduction block. Activation times (in milliseconds) of selected regions are indicated. Esyn = electrical synchrony index (mean activation time difference between lateral RV and LV free walls); smaller absolute value corresponds to greater synchrony. RVB, right ventricular breakthrough; QRSd, QRS duration. (From Jia *et al.*[24] Reproduced by permission.)**

leads, improving electrical synchrony. In contrast, anterior LV lead placement does not improve electrical synchrony due to regions of block and slow conduction in the antero-lateral aspects, which interfere with anterior to lateral wall propagation.

Summary

Cardiac arrhythmias are a major cause of death and disability. There is clearly a need for a noninvasive imaging modality, equivalent to CT or MRI,

for cardiac electrophysiology and arrhythmia. The examples provided here demonstrate the ability of ECGI to image noninvasively various electrical activity patterns on the surface of the heart. This capability could help in (1) screening of people for risk of life threatening arrhythmias; (2) specific diagnosis of arrhythmia mechanisms to facilitate specific therapy; (3) determination of arrhythmogenic substrate and its location to guide targeted intervention (e.g. ablation, pacing, CRT, drug delivery, and gene transfer); (4) follow up and evaluation of therapy. In addition, it could be used as a research tool to study mechanisms of arrhythmias in humans, where the electrophysiological substrate is markedly different from animal models used in arrhythmia research.

Acknowledgments

The work summarized here was supported by a Merit Award R37-HL33343 and Grant R01-HL49054 from the NIH-National Heart, Lung and Blood Institute. Yoram Rudy is the Fred Saigh Distinguished Professor at Washington University in St. Louis. I extend thanks to Kimberly Smith for her help in preparing this manuscript.

Conflicts of interest

Yoram Rudy chairs the scientific advisory board and holds equity in CardioInsight Technologies (CIT). CIT does not support any research conducted by Dr. Rudy, including that presented here.

References

1. Ramanathan, C., R.N. Ghanem, P. Jia, *et al*. 2004. Noninvasive electrocardiographic imaging for cardiac electrophysiology and arrhythmia. *Nat. Med*. **10:** 422–428.
2. Oster, H.S., B. Taccardi, R.L. Lux, *et al*. 1997. Noninvasive electrocardiographic imaging: reconstruction of epicardial potentials, electrograms, and isochrones and localization of single and multiple electrocardiac events. *Circulation* **96:** 1012–1024.
3. Oster, H.S., B. Taccardi, R.L. Lux, *et al*. 1998. Electrocardiographic imaging: noninvasive characterization of intramural myocardial activation from inverse-reconstructed epicardial potentials and electrograms. *Circulation* **97:** 1496–1507.
4. Burnes, J.E., B. Taccardi, R.S. MacLeod & Y. Rudy. 2000. Noninvasive ECG imaging of electrophysiologically abnormal substrates in infarcted hearts: a model study. *Circulation* **101:** 533–540.
5. Burnes, J.E., B. Taccardi, P.R. Ershler & Y. Rudy. 2001. Noninvasive electrocardiographic imaging of substrate and intramural ventricular tachycardia in infarcted hearts. *J. Am. Coll. Cardiol.* **38:** 2071–2078.
6. Ghanem, R.N., J.E. Burnes, A.L. Waldo & Y. Rudy. 2001. Imaging dispersion of myocardial repolarization. II: Noninvasive reconstruction of epicardial measures. *Circulation* **104:** 1306–1312.
7. Ghanem, R.N., P. Jia, C. Ramanathan, *et al*. 2005. Noninvasive electrocardiographic imaging (ECGI): comparison to intraoperative mapping in patients. *Heart Rhythm* **2:** 339–354.
8. Rudy, Y. & B.J. Messinger-Rapport. 1988. The inverse problem in electrocardiography: solutions in terms of epicardial potentials. *Crit. Rev. Biomed. Eng.* **16:** 215–268.
9. Brebbia, C.A., J.C.F. Telles & L.C. Wrobel. 1984. *Boundary Element Techniques: Theory and Applications in Engineering*. Springer-Verlag. Berlin.
10. Tikhonov, A.N. & V.Y. Arsenin. 1977. *Solutions of Ill-posed Problems*. Wiley. New York.
11. Ramanathan, C., P. Jia, R. Ghanem, *et al*. 2003. Noninvasive electrocardiographic imaging (ECGI): application of the generalized minimal residual (GMRes) method. *Ann. Biomed. Eng.* **31:** 981–994.
12. Ramanathan, C., P. Jia, R.N. Ghanem, *et al*. 2006. Activation and repolarization of the normal human heart under complete physiological conditions. *Proc. Nat. Acad. Sci. USA* **103:** 6309–6314.
13. Spach, M.S., R.C. Barr, *et al*. 1977. Origin of body surface QRS and T wave potentials from epicardial potential distributions in the intact chimpanzee. *Circulation* **55:** 268–268.
14. Durrer, D., R.T. van Dam, G.E. Freud, *et al*. 1970. Total excitation of the isolated human heart. *Circulation* **41:** 899–912.
15. Wang, Y., R. Schuessler, R. Damiano, *et al*. 2007. Noninvasive electrocardiographic imaging (ECGI) of scar-related atypical atrial flutter. *Heart Rhythm.* **12:** 1565–1567.
16. Yamabe, H., I. Misumi, H. Fukushima, *et al*. 2002. Conduction properties of the crista terminalis and its influence on the right atrial activation sequence in patients with typical atrial flutter. *Pacing Clin. Electrophysiol.* **25:** 132–141.
17. Daoud, E.G. & F. Morady. 1998. Pathophysiology of atrial flutter. *Annu. Rev. Med.* **49:** 77–83.
18. Rodriguez, L.M., C. Timmermans, A. Nabar, *et al*. 2001. Biatrial activation in isthmus-dependent atrial flutter. *Circulation* **104:** 2545–2550.

19. Ghosh, S., E. Rhee, J. Avari, *et al*. 2008. Cardiac memory in patients with Wolff-Parkinson-White syndrome: Noninvasive imaging of activation and repolarization before and after catheter ablation. *Circulation* **108:** 907–915.
20. Ghosh, S., E. Rhee, J. Avari, *et al*. 2007. Noninvasive Electrocardiographic Imaging (ECGI) of a univentricular heart with Wolff-Parkinson-White Syndrome. *Heart Rhythm* **4:** 605–6087.
21. Pappone, C., V. Santinelli, F. Manguso, *et al*. 2003. A randomized study of prophylactic catheter ablation in asymptomatic patients with the Wolff-Parkinson-White syndrome. *N. Engl. J. Med*. **349:** 1803–1811.
22. Rosenbaum, M.B., H.H. Blanco, M.V. Elizari, *et al*. 1982. Electrotonic modulation of the T wave and cardiac memory. *Am. J. Cardiol*. **50:** 213–222.
23. Rosen, M.R. & I. Cohen. 2005. Cardiac memory: new insights into molecular mechanisms. *J. Physiol*. **570:** 209–2185.
24. Jia, P., C. Ramanathan, R.N. Ghanem, *et al*. 2006. Electrocardiographic imaging of cardiac resynchronization therapy in heart failure: observation of variable electrophysiologic responses. *Heart Rhythm* **3:** 296–310.